

Radial Velocities of Newly Discovered Globular Clusters in NGC 5128

Kristin A. Woodley¹

Department of Physics & Astronomy, McMaster University, Hamilton ON L8S 4M1

`woodleka@physics.mcmaster.ca`

William E. Harris¹

Department of Physics & Astronomy, McMaster University, Hamilton ON L8S 4M1

`harris@physics.mcmaster.ca`

Gretchen L. H. Harris

Department of Physics, University of Waterloo, Waterloo ON N2L 3G1

`glharris@astro.uwaterloo.ca`

ABSTRACT

We present radial velocity measurements for 74 globular clusters (GCs) in the nearby giant elliptical NGC 5128, of which 31 are newly discovered clusters. All the GC candidates were taken from the list of possible new clusters given in the Harris, Harris, & Geisler (2004) photometric survey. In addition to the newly confirmed clusters, we identified 24 definite foreground stars and 31 probable background galaxies. From a combined list of 299 known GCs in NGC 5128 with measured radial velocities and metallicity-sensitive ($C - T_1$) photometric indices, we construct a new metallicity distribution function (MDF) for the cluster system. The MDF shows an approximately bimodal form, with centroids at $[\text{Fe}/\text{H}] = -1.46$ and -0.53 , and with nearly equal numbers of metal-poor and metal-rich clusters in the two modes. However, there are many intermediate-color clusters in the distribution, and the fainter clusters tend to have a higher proportion of red clusters. These features of the MDF may indicate a widespread age range within the cluster system as well as an intrinsically broad metallicity spread.

Subject headings: galaxies: elliptical and lenticular, cD — galaxies: individual (NGC 5128) — globular clusters: general — techniques: radial velocities

¹Visiting Observer, Cerro Tololo Interamerican Observatory, Operated by the Association of Universities for Research in Astronomy, Inc. (AURA) under cooperative agreement with the National Science Foundation.

1. Introduction

Globular clusters (GCs) are simple stellar populations (single age, single metallicity) that help to trace the formation history of their host galaxy. GCs are also powerful tools in revealing the halo kinematics and dynamics, if large samples of globular cluster radial velocities can be obtained.

NGC 5128, the central galaxy in the Centaurus cluster 3.9 Mpc away, and the nearest readily accessible giant E galaxy, provides a unique and exciting possibility to study the dynamics and formation history through its globular cluster system (GCS). However, finding its clusters individually is a difficult job: at its moderately low Galactic latitude of 19° , field contamination by both foreground stars and background galaxies is significant, and the GCs cannot be distinguished by only image morphology, object size, or color. Thus except for the very expensive and time-consuming approach of resolving the GCs into individual stars by (say) HST imaging, radial velocity determinations provide the only definitive method for classifying a candidate object in the NGC 5128 field as a genuine GC.

NGC 5128 has a statistically determined total population of 980 ± 120 globular clusters, giving it a low specific frequency $S_N = 1.4 \pm 0.2$ (Harris, Harris, & Geisler 2004, hereafter HHG04). An S_N value this low (in the range occupied by large spiral galaxies) is suggestive of a merger origin (Harris 2001); other indicators of mergers are the faint isophotal shells in the halo of the galaxy (e.g. Peng et al. 2002), and the activity in the inner 5 kpc region indicated by the visible dust lane, the recent star formation, and the presence of gas. The GCS, with its wide mixture of cluster metallicities and perhaps ages, should provide many additional clues to the formation history surrounding this giant elliptical. An excellent starting point for any such discussion is to have as large as possible a list of individual, certainly identified GCs through radial velocity measurements.

Previous work has led to a list of 215 confirmed GCs in NGC 5128 with radial velocity measurements (Peng, Ford, & Freeman 2004, hereafter PFF04). Many hundreds more clusters remain to be found. In this paper, the first of a new series of studies of the GCS in this unique galaxy, we present new velocity measurements and the discovery of 31 new GCs.

2. Data Reduction and Velocity Measurements

The wide-field photometry study of the NGC 5128 field in the Washington CMT_1 system by Harris et al. (2004) provides a list of 327 GC candidates having globular-cluster-like colors and slightly nonstellar morphology. This list provides the basis for our new radial velocity survey.

2.1. Observations and Data Reduction

Observations were taken at the Cerro Tololo Inter-American Observatory (CTIO) 4m telescope in April 2004. The Hydra multi-object fibre-fed spectrograph, with 40' diameter field of view, was used with the KPGL1 grating and $2\times$ binning in dispersion, giving a spectral resolution element of approximately 3.5 binned pixels (FWHM). The spectral coverage was $\lambda 3900 \text{ \AA} - \lambda 5300 \text{ \AA}$, extending from Ca II H+K at the blue end to the Mgb features at the red end at 1.18 \AA/px . Of our three assigned nights, two were lost to clouds, and the third had poor seeing throughout ($2'' - 3''$). Nevertheless, we successfully observed two Hydra field configurations, both centered on the galaxy. Total exposure times were $6 \times 1800 \text{ sec}$ for the first field and $7 \times 1800 \text{ sec}$ for the second.

The data reduction was performed through the *dohydra* package within IRAF¹, following the normal sequence of preprocessing described on the Hydra webpages. The raw images were overscan and bias subtracted, and the detector was flat-fielded with milk flats (daytime sky exposures) using a diffusing filter in front of the Hydra fibres. Cosmic rays were subtracted with a Laplacian edge detection method (van Dokkum 2001). Spectral throughput and dispersion corrections were applied based on the standard continuum lamp and Hydra HeNeAr penray lamp to obtain wavelength calibrated spectra.

2.2. Background Light Removal

Removal of background light from each object spectrum includes both the uniform dark-sky illumination and (for the GC candidates close to the galaxy center) the bulge light from NGC 5128 itself. To trace both effects, we placed 40-50 fibers in each Hydra field configuration on blank-sky positions sprinkled across the entire field, then plotted the mean intensity of each sky fiber versus radius from galaxy center. The data showed that the bulge light profile was well matched by a $(1/r^2)$ radial dependence (see, e.g. Harris, Harris, & Geisler 2004).

For radii larger than $r \simeq 11'$, the galaxy bulge light contamination was negligible and we simply subtracted the average of the sky spectra at these larger radii from all the object spectra. For the inner objects, we then removed the additional bulge light contamination through appropriate radial scaling of the average bulge sky spectrum.

2.3. Radial Velocities

From the fully preprocessed and background-subtracted spectra, we derived radial velocities obtained through Fourier cross-correlation, using the *fxcor* task in the *radial velocity* IRAF package.

¹IRAF is distributed by the National Optical Astronomy Observatory, which is operated by the Association of Universities for Research in Astronomy Inc., under cooperative agreement with the National Science Foundation.

The spectrum of each candidate object was correlated against a template spectrum of known velocity and the correlation peak was fit with a Lorentzian function. Our template spectrum was constructed from the sum of five of the previously known bright GCs in NGC 5128 (C7, C11, C17, C19, and C20), which we observed in both of our Hydra fields and which have well determined velocities taken from PFF04. Thus, the template was very well tuned to the spectral features in the GCs that we are searching for since it was built from exactly the same type of object.

3. Results

3.1. Candidate Distribution

NGC 5128 has a systemic velocity of 541 km s^{-1} (Hui et al. 1995) and an internal stellar velocity dispersion of $\sim 140 \text{ km s}^{-1}$ (Wilkinson et al. 1986). These features allow a clean velocity separation between GCs and foreground stars in the Milky Way or background galaxies. As shown (e.g.) by PFF04, the foreground stars have velocities almost all less than $\sim 200 \text{ km s}^{-1}$, while any faint background galaxies will have velocities of many thousands of km s^{-1} . Any objects that fall in the range $200 < v_r < 1000 \text{ km s}^{-1}$ (and drawn from the candidate list pre-selected by image morphology, magnitude and color) will therefore be near-certain GCs.

From both Hydra fields combined, we obtained radial velocity measurements for 86 candidate GCs and 43 previously known GCs. The previously known clusters were used to help establish the zero point of our velocity scale and check the internal measurement uncertainties (see below). Of the candidates, we found 31 with $240 \leq v_r \leq 900 \text{ km s}^{-1}$, which we identify as newly discovered GCs. Of these 31, 5 are X-ray sources previously detected by Kraft et al. (2001). In Table 1, we list the data for these GCs. Successive columns give the identification number (WHH prefixes denote our new objects), coordinates, radial distance from the center of NGC 5128, V and $(C - T_1)$ photometry from HHG04, radial velocity, and velocity uncertainty from the *fxcor* solution.

Of the 55 remaining candidates, 24 are definite foreground stars with $-91 \leq v_r \leq 110 \text{ km s}^{-1}$, and 31 are likely background galaxies; these are listed in Table 2. The objects with null results for the radial velocity are ones whose spectra had a poor correlation with the GC template spectrum, suggestive of a background galaxy with either very large redshift or spectral features very different from the template. Confirming 31 candidates as GCs out of the 86 candidates observed yields an encouraging 36% hit rate given the extremely high field contamination level, and demonstrates the value of rigorous preselection by color and object morphology (see the discussion of HHG04).

Table 3 lists the resulting radial velocity measurements of the 43 previously known GCs re-measured in this study. The identification number prefixes C, G, or pff_gc are originally listed by Harris et al. (1992) and PFF04.

Figure 1 shows the locations of the newly confirmed and previously known GCs. Whereas most previous surveys have concentrated on fields along the isophotal major axis of NGC 5128 (along

a line running SW to NE), it is worth noting that many of our newly identified GCs lie along the less well studied minor axis parallel to the inner dust lane. There are likely to be many more to be found still. Figure 2 shows the velocity distribution of the GCs and foreground stars measured from this study; the two types of objects are clearly distinguished by radial velocity at $v_r \sim 200$ km s⁻¹.

The analysis of the GCS radial profile by HHG04 showed that the majority of GCs lie within $r = 15'$ from the galaxy center, with the main contribution of the clusters residing in an even more compact environment within $r = 10'$. Our new sample of 31 GCs has a median value of $r = 8.25'$.

The mean radial velocity difference between the previously known clusters in our study and those of PFF04 is less than 10 km s⁻¹, well within the standard deviation of the mean (see below). The zero point of our velocity scale therefore needs no adjustment.

3.2. Comments on Individual Objects

The raw spectra of clusters WHH-12, WHH-25, WHH-31, pff_gc-073, and the non-GC candidates 100, 133, and 136 had a few intensity spikes that could not be removed in the preprocessing stage. These regions were artificially removed before the cross-correlation solutions, resulting in higher than normal velocity uncertainties (see Tables 1 & 2).

For the previously known cluster C10, we measure $v_r = 855 \pm 33$ km s⁻¹. This differs quite a bit from the PFF04 measurement of 522 ± 53 km s⁻¹, but it agrees well with Hesser, Harris, & Harris (1986) (770 km s⁻¹) and also with the new measurement from Beasley et al. (2005) (836 km s⁻¹). We therefore believe our measurement to be in the correct range.

There is one candidate for which the velocity solution revealed a second correlation peak only slightly smaller than the highest peak that is automatically found and fit by the *fxcor* task. For WHH-22, the highest correlation peak yields $v_r = 492 \pm 126$ km s⁻¹, clearly classifying this object as a GC; but a second peak yields $v_r \sim 20$ km s⁻¹, which would classify it as a foreground star. Visual inspection of the candidate spectrum shows hydrogen and calcium line strengths consistent with those for clusters. We keep this object as a probably GC, but with these uncertainties in mind. A strong secondary peak was also revealed for the known cluster, pff_gc-060. The highest peak gives $v_r = 818 \pm 96$ km s⁻¹, but a second peak gives 217 km s⁻¹, which would put it on the borderline between GCs and foreground stars. Its spectrum does not have high enough signal-to-noise to determine upon visual inspection whether or not it is a cluster. However, this object has been measured by PFF04 to have $v_r = 893 \pm 19$ km s⁻¹, agreeing with our highest peak correlation value.

For three previously known GCs, C21, pff_gc-089, and pff_gc-064, the highest correlation peak fit generated by *fxcor* yielded radial velocities that were inconsistent with previous measurements. A closer look at the correlated spectra shows a second strong correlation peak in all cases. Choosing

the secondary peak gave $v_r = 461 \pm 96 \text{ km s}^{-1}$ for C21 (compared with $465 \pm 7 \text{ km s}^{-1}$ from PFF04) and $v_r = 553 \pm 103 \text{ km s}^{-1}$ for pff_gc-089 (compared with $v_r = 502 \pm 61 \text{ km s}^{-1}$ from PFF04). C21 has also been previously measured by Hesser, Harris, & Harris (1986) to be at $v_r = 490 \text{ km s}^{-1}$. For these two objects we therefore adopted the second correlation peaks. The known cluster, pff_gc-064, measured in both field configurations, presents a slightly different problem: the initial poorly correlated fit in field 1 nominally classified it as a possible background galaxy. Yet, there is a second strong correlation peak with $v_r = 548 \pm 97 \text{ km s}^{-1}$, agreeing with the field 2 result for the same object of $563 \pm 84 \text{ km s}^{-1}$ and also with the PFF04 measurement of $v_r = 557 \pm 31 \text{ km s}^{-1}$.

There are three other candidates measured in both field configurations, 43/44, 109/110, and 101. Their radial velocities classified these objects as possible background galaxies, with their averaged radial velocities as displayed in Tables 2. Objects 43 and 44 in the candidate list of HHG04 turn out to be the same object, and similarly candidates 109 and 110 are the same. Lastly, we note that 12 of the HHG04 candidate objects measured in this study turned out to be previously known GCs. These objects are listed in Table 4.

3.3. Velocity Measurement Uncertainties

The radial velocity uncertainties we quote in the tables are from the *fxcor* solutions. Generally, these are well correlated with the object’s apparent magnitude and thus the signal-to-noise of the spectra. Figure 4 shows the nominal radial velocity uncertainties plotted versus V magnitude. The new GCs (excluding WHH-12, WHH-25, and WHH-31; see above) with $V < 18.5$ had a mean $\sigma(v_r) = \pm 32 \text{ km s}^{-1}$ and $S/N = 13$ per pixel in the continuum region near $\lambda 4525\text{\AA}$. For $V \geq 18.5$, the mean uncertainty was $\sigma(v_r) = \pm 74 \text{ km s}^{-1}$ and $S/N (\lambda 4525\text{\AA}) = 4.5$ per pixel.

We tested the *fxcor* uncertainties in several ways. First, the comparison between our velocities and those of PFF04 for 42 clusters in common (excluding C10 as mentioned above) is shown in Figure 3. The standard deviation of the differences between the two studies was $\pm 44.5 \text{ km s}^{-1}$. If the two studies have comparable internal uncertainties, then this suggests that for GCs brighter than $V \simeq 19$ the typical uncertainty of our measurements is no larger than $\pm 30 \text{ km s}^{-1}$, in agreement with the *mknoise* simulations in Fig. 4 (see below).

Another internal test was to compare the velocities for objects that we measured in both Hydra field settings. There were 13 such GCs measured twice, 12 of them brighter than $V = 19$: C2, C6, C13, C14, C18, C19, C20, C26, C37, C38, C44, pff_gc-056, and pff_gc-064 ($V = 19.80 \text{ mag}$). For these, the mean velocity difference between the two fields was 3.9 km s^{-1} , with a standard deviation of $\pm 22.3 \text{ km s}^{-1}$, again consistent with Fig. 4.

Finally, we compared the *fxcor* uncertainties with those generated from simulated noisy spectra, adding Gaussian noise to the template spectrum with the IRAF *artdata.mknoise* task. Several dozen of these artificial spectra were cross-correlated against the original template spectrum and the resulting radial velocity uncertainties plotted against the S/N for each noisy spectrum. The

results verify that for $S/N > 5$ per pixel (corresponding roughly to $V < 18.5$), the velocity uncertainty was smaller than $\pm 30 \text{ km s}^{-1}$. Fainter than this, the uncertainty rises exponentially, reaching $\pm 100 \text{ km s}^{-1}$ at $S/N \simeq 2$ per pixel (or $V \sim 20$). In Fig. 4, the solid line shows the velocity uncertainty increasing with V magnitude, from the *mknoise* simulations. This ideal line is the minimum uncertainty due only to random noise, providing a lower boundary to the observed uncertainties.

In summary, we find that the results generated by *fxcor* (with its uncertainties as listed in Tables 1, 2, & 3) provide estimates of the internal velocity uncertainties that are quite close to the estimates from simulations and from comparisons with previous data. This may in large part be because we deliberately used a standard velocity template which accurately matches the program objects. We conclude that the internal uncertainties of our measured velocities are near $\pm 20 \text{ km s}^{-1}$ for the very brightest clusters, increasing to $\pm 100 \text{ km s}^{-1}$ for the ones at $V \sim 20$ or fainter.

4. The Metallicity Distribution Function

A new analysis of the radial velocities and kinematics of the confirmed GCS in NGC 5128, with a much enlarged cluster sample over that used in PFF04, will be discussed in a later paper (Woodley et al. 2005). For the present, we provide here only a brief discussion on the metallicity distribution function (MDF).

The top panel in Figure 5 shows the MDF for a total of 299 GCs in NGC 5128 that are radial-velocity members *and* that have available $(C - T_1)$ photometric indices: 168 are previously confirmed clusters (PFF04), 31 are the new clusters from this study, and 100 more are from the upcoming study of Beasley et al. (2005). Although there are a few dozen other highly probable GCs that have recently been found in NGC 5128 from image morphology studies (Rejkuba 2001; Harris et al. 2002; Gomez et al. 2005), we restrict the current discussion to an almost certainly “pure” sample generated by the combination of object color, morphology, and radial velocity.

The dereddened colors $(C - T_1)_0$ from HHG04 were transformed to $[\text{Fe}/\text{H}]$ through the conversion derived by Harris & Harris (2002) calibrated through the Milky Way cluster data. We adopt a foreground reddening value of $E(B - V) = 0.11$ for NGC 5128, corresponding to $E(C - T_1) = 0.22$. Because the transformation is slightly nonlinear, the uncertainty in $[\text{Fe}/\text{H}]$ is a function of metallicity. For a typical color uncertainty $\sigma(C - T_1) \simeq 0.1$, the corresponding uncertainty in $[\text{Fe}/\text{H}]$ is near ± 0.2 dex at the metal-poor end, decreasing to ± 0.07 dex at the metal-rich end.

The MDF, binned in steps of $\Delta[\text{Fe}/\text{H}] = 0.10$, is shown in Figure 5, along with the same distribution for the Milky Way clusters (data from Harris 1996). As has been found in all previous studies of NGC 5128 starting with Harris et al. (1992), the MDF is extremely broad and populated by roughly equal numbers of metal-poor and metal-rich clusters. The color bimodality of NGC 5128 has recently been confirmed by Peng, Ford, & Freeman (2004) in 4 different photometric indices. They used spectroscopic line indices of $H\beta$ versus $[\text{MgFe}]'$ to suggest the blue GC population was metal-poor and old (8 – 15 Gyr) and the red GC population was metal-rich and young (mean age

$\sim 5_{-2}^{+3}$ Gyr). A bimodal-Gaussian distribution (shown in Fig. 5) provides a reasonable fit to the total MDF, but not as cleanly as in many other giant galaxies including the Milky Way (plotted for comparison in the lower panel of the figure). The fit of the bimodal model to the MDF is not well constrained, allowing a wide range of particular combinations of Gaussians. The two centroids shown, at $[\text{Fe}/\text{H}] = -1.46$ and -0.53 , are similar to the fit obtained by HHG04 (see their Figure 10) from a smaller cluster sample. The metal-poor part of our entire sample makes up $\sim 54\%$ of the total population and the metal-rich part $\sim 46\%$, in close agreement with HHG04. It does not seem likely that internal differential reddening of the clusters is an important factor in creating the color spread, since reddening-generated differences in color of several tenths of a magnitude would be needed to move a cluster from the metal-poor mode to (e.g.) $[\text{Fe}/\text{H}] \sim -1$, yet all the objects with $(C - T_1)$ photometry lie clearly outside the dust lane and into the clear regions of the bulge and halo (see Harris et al. 2004, for extensive discussion).

As has long been realized, the Milky Way MDF (bottom panel in Figure 5) provides a clean match to the bimodal-Gaussian model, with peaks at $[\text{Fe}/\text{H}] = -1.58 \pm 0.05$ and -0.64 ± 0.07 . The standard deviations are 0.32 and 0.23 for the metal-poor and metal-rich subpopulations, both narrower than their counterparts for NGC 5128. Both centroids are slightly but noticeably more metal-poor than those in NGC 5128.

By comparison, the MDF of the M31 globular clusters shows $[\text{Fe}/\text{H}]$ peaks that are more similar to NGC 5128. Perrett et al. (2002) find M31 centroids of $[\text{Fe}/\text{H}] = -1.44 \pm 0.03$ and -0.50 ± 0.04 . Thus, it is likely that if NGC 5128 is a product of major mergers, then it would need M31-sized galaxies as progenitors, rather than systems like the Milky Way which have lower-metallicity clusters.

If we assume that NGC 5128 was built through a series of mergers extending for several Gigayears, then the GCS might contain a wide range of ages. Thus the MDF shown here, based on photometric metallicities from $(C - T_1)$ with the assumption that all the clusters are homogeneously old, would underestimate the true metallicity of younger clusters. This effect would artificially increase the spread in the MDF and partially blur out a distribution that was intrinsically bimodal. The classic age/metallicity degeneracy for broad band colors prevents us from distinguishing this alternative from an intrinsically broad, even MDF.

Figure 6 displays the NGC 5128 sample divided into bright ($V \leq 19.5$) and faint ($V > 19.5$) clusters. Interestingly, the fainter sample appears to have a higher proportion of metal-rich clusters than the brighter sample. A direct least-squares correlation of $[\text{Fe}/\text{H}]$ versus V magnitude shows no significant trend within the larger scatter in $[\text{Fe}/\text{H}]$. It is possible that we are simply seeing an intrinsically broad and uniform spread of cluster metallicities, in which the younger and more metal-rich ones tend to be of somewhat lower mass or luminosity, consistent with the age differences suggested by PFF04. A wide range of ages would further increase the apparent spread of the MDF as seen in Fig. 6.

Further spectroscopic studies and more detailed modelling will be needed to test these spec-

ulations. In later analyses (Woodley et al. 2005; Beasley et al. 2005) we will discuss the age distributions and kinematics of the cluster system further.

In Figure 7, the cluster metallicities are displayed as a function of projected galactocentric radius. Both metal-poor ($[\text{Fe}/\text{H}] > -1.0$) and metal-rich ($[\text{Fe}/\text{H}] < -1.0$) clusters have been found extending out to a radius of $40'$ (~ 45 kpc). However, beyond $r \sim 20'$, there are double the number of metal-poor compared to metal-rich clusters. The mean metallicity beyond this distance is $[\text{Fe}/\text{H}] = -1.21$ with a standard deviation of 0.47. As is discussed in more detail in HHG04, this change in ratios of subpopulations is not likely to be due to selection bias and is therefore probably intrinsic to the system.

5. Summary

We present new radial velocities for 86 globular cluster candidates selected from Harris, Harris, & Geisler (2004). The results show 31 newly identified clusters with $240 \leq v_r \leq 900 \text{ km s}^{-1}$, 24 definite foreground stars with $-91 \leq v_r \leq 110 \text{ km s}^{-1}$, and 31 probable background galaxies. We also obtained velocities for 43 previously known GCs in NGC 5128. The internal uncertainty in our v_r measurements ranges from $\pm 20 \text{ km s}^{-1}$ at the bright end of the sample ($V < 18$) to $\sim \pm 100 \text{ km s}^{-1}$ at $V \sim 20$.

Combining our data with previously published material, we derive a metallicity distribution for the GCs based on 299 clusters. A bimodal distribution with centroids at $[\text{Fe}/\text{H}] = -1.46$ and -0.53 provides an approximate fit to the MDF, though not highly accurate, and the data hint that the relative proportions of metal-poor and metal-rich clusters may change with luminosity. Two possible interpretations are that (a) we may be seeing the combined effects of a several-Gy internal age spread in the cluster system, combined with a trend for the younger clusters to be progressively less massive, or (b) the MDF is genuinely broad and evenly distributed, unlike the more cleanly bimodal MDFs seen in other giant galaxies.

We greatly appreciate the data reduction advice and support provided by Knut Olsen at CTIO, and also advice regarding uncertainty tests from David James at Vanderbilt University. We thank Mike Beasley for transmitting cluster velocity data in advance of publication. This work was supported by the Natural Sciences and Engineering Research Council of Canada through research grants to GLHH and WEH.

REFERENCES

- Beasley, M. et al. 2005, in preparation
 Gomez, M. et al. 2005, in preparation

- Harris, G.L.H., Geisler, D., Harris, H.C., & Hesser, J.E. 1992, *AJ*, 104, 613
- Harris, G.L.H., Geisler, D., Harris, W.E., Schmidt, B.P., Hesser, J.E., Reid, M., Milne, M., Hulme S.C., & Kidd, T.T. 2004, *AJ*, 128, 712
- Harris, G.L.H., Harris, W.E., & Geisler, D. 2004, *AJ*, 128, 723 (HHG04)
- Harris, W.E. 1996, *AJ*, 112, 1487
- Harris, W.E. 2001, in *Star Clusters*, Saas-Fee Advanced Course 28 (New York: Springer), ed. L. Labhardt & B. Binggeli
- Harris, W.E. & Harris, G.L.H. 2002, *AJ*, 123, 3108
- Harris, W.E., Harris, G.L.H., Holland, S.T., & McLaughlin, D.E. 2002, *AJ*, 124, 1435
- Hesser, J.E., Harris, H.C., & Harris, G.L.H. 1986, *ApJ*, 303, L51
- Hui, X., Ford, H.C., Freeman, K.C., & Dopita, M.A. 1995, *ApJ*, 449, 592
- Kraft, R.P., Kregenow J.M., Forman, W.R., Jones, C., & Murray, S.S. 2001, *ApJ*, 560, 675
- Peng, E.W., Ford, H.C., & Freeman, K.C. 2004, *ApJS*, 150, 367 (PPF04)
- Peng, E.W., Ford, H.C., & Freeman, K.C. 2004, *ApJ*, 602, 705
- Peng, E.W., Ford, H.C., Freeman, K.C., & White, R.L. 2002, *AJ*, 124, 3144
- Perrett, K.M., Bridges, T.J., Hanes, D.A., Irwin, M.J., Brodie, J.P., Carter, D., Huchra, J.P., & Watson, F.G. 2002, *AJ*, 123, 2490
- Rejkuba, M. 2001, *A&A*, 369, 812
- van den Bergh, S., Hesser, J.E., & Harris, G.L.H. 1981, *AJ*, 86, 24
- van Dokkum, P.G. 2001, *PASP*, 113, 1420
- Wilkinson, A., Sharples, R.M., Fosbury, R.A.E., & Wallace, P.T. 1986, *MNRAS*, 218, 297
- Woodley, K.A. et al. 2005, in preparation

Table 1. Radial Velocity Measurements for Globular Clusters

Cluster	RA (J2000)	Dec (J2000)	R_{gc} (arcmin)	V (mag)	(C-T ₁)	v_r (km s ⁻¹)	$\sigma(v_r)$ (km s ⁻¹)
WHH-1	13 24 21.40	-43 02 36.8	12.19	18.23	1.484	600	35
WHH-2	13 24 23.98	-42 54 10.7	13.56	19.87	1.270	582	81
WHH-3	13 24 32.17	-43 10 56.9	14.10	19.59	1.470	636	78
WHH-4	13 24 40.60	-43 13 18.1	14.89	19.13	1.927	685	43
WHH-5	13 24 44.58	-43 02 47.3	8.04	19.50	1.386	671	41
WHH-6	13 24 47.37	-42 57 51.2	8.06	19.75	1.931	712	67
WHH-7 ^a	13 25 05.02	-42 57 15.0	5.68	17.43	1.863	722	20
WHH-8 ^a	13 25 07.62	-43 01 15.2	3.66	18.05	2.026	690	32
WHH-9	13 25 08.51	-43 02 57.4	3.93	18.90	1.979	315	100
WHH-10	13 25 12.84	-42 56 59.8	4.95	19.70	1.334	664	141
WHH-11 ^a	13 25 14.24	-43 07 23.5	6.71	19.55	2.066	562	55
WHH-12	13 25 18.27	-42 53 04.8	8.25	19.31	1.521	558	99 ^b
WHH-13	13 25 21.29	-42 49 17.7	11.91	19.34	1.854	467	47
WHH-14	13 25 25.49	-42 56 31.2	4.64	20.28	1.300	436	80
WHH-15	13 25 26.78	-42 52 39.9	8.48	20.13	1.153	506	57
WHH-16 ^a	13 25 27.97	-43 04 02.2	2.89	19.20	2.036	749	80
WHH-17	13 25 29.25	-42 57 47.1	3.38	18.73	1.409	588	127
WHH-18	13 25 30.07	-42 56 46.9	4.39	18.48	1.752	771	31
WHH-19	13 25 31.03	-42 50 14.9	10.92	17.51	1.177	470	49
WHH-20	13 25 34.36	-42 51 05.9	10.12	19.19	1.517	242	54
WHH-21	13 25 35.22	-43 12 01.5	10.97	19.22	0.994	243	61
WHH-22 ^a	13 25 35.31	-43 05 29.0	4.56	18.63	1.631	492 ^c	126
WHH-23	13 25 45.90	-42 57 20.2	5.07	18.60	1.137	286	63
WHH-24	13 25 46.00	-42 56 53.0	5.43	19.85	1.288	566	48
WHH-25	13 25 50.34	-43 04 08.2	5.12	20.17	1.621	551	95 ^b
WHH-26	13 25 56.59	-42 51 46.6	10.76	19.16	1.762	412	36
WHH-27	13 26 12.82	-43 09 09.2	11.51	18.73	1.885	545	60
WHH-28	13 26 14.18	-43 08 30.4	11.25	19.32	1.414	506	123
WHH-29	13 26 22.08	-43 09 10.7	12.79	19.98	1.538	505	78
WHH-30	13 26 23.60	-43 03 43.9	10.55	19.56	1.488	470	66
WHH-31	13 26 41.43	-43 11 25.0	16.96	19.65	1.618	573	67 ^b

Table 1—Continued

Cluster	RA (J2000)	Dec (J2000)	R_{gc} (arcmin)	V (mag)	(C-T ₁)	v_r (km s ⁻¹)	$\sigma(v_r)$ (km s ⁻¹)
---------	---------------	----------------	----------------------	------------	---------------------	--------------------------------	--

^aDetected as X-ray source from Kraft et al. (2001)

^bRegions of spectrum affected by cosmic ray spikes were masked out during correlation.

^cStrong secondary correlation peaks.

Table 2. Foreground Stars and Background Galaxies

ID	R.A. (J2000)	Dec. (J2000)	v_r (km s ⁻¹)	$\sigma(v_r)$ (km s ⁻¹)	Comments
36	13 24 02.55	-42 49 29.4	64	42	star
3	13 24 28.96	-43 10 58.3	-24	23	star
8	13 24 52.11	-43 08 24.3	-1	26	star
19	13 24 56.46	-43 06 34.7	-46	24	star
11	13 25 04.20	-43 02 29.3	-30	26	star
14	13 25 08.59	-43 07 43.4	-17	47	star
13	13 25 10.06	-43 07 40.7	-30	21	star
26	13 25 17.79	-43 13 05.6	-70	42	star
25	13 25 24.37	-43 12 23.1	-13	23	star
62	13 25 25.10	-43 12 27.0	-82	79	star
27	13 25 42.62	-43 10 21.4	-20	32	star
77	13 25 47.98	-43 00 57.6	106	106	star
4	13 25 55.77	-43 03 00.9	18	21	star
1	13 25 56.40	-42 59 37.3	40	23	star
2	13 25 57.38	-42 59 48.5	1	22	star
6	13 25 58.39	-42 55 27.6	-22	21	star
23	13 25 58.44	-43 03 06.4	-3	25	star
20	13 26 10.41	-43 00 53.6	-11	26	star
73	13 26 15.41	-42 57 46.8	3	118	star
56	13 26 17.81	-43 00 29.7	-60	37	star
17	13 26 20.74	-43 09 13.2	51	33	star
89	13 26 21.11	-43 03 08.2	-85	99	star
61	13 26 32.79	-43 02 59.4	31	50	star
38	13 26 33.08	-43 03 14.0	-91	40	star
283	13 24 04.50	-42 48 16.2	47636	81	galaxy
285	13 24 05.49	-42 47 24.1	4729	124	galaxy
290	13 24 13.26	-42 57 42.1	-	-	PC ^c
94	13 24 28.15	-42 53 04.6	35382	178	galaxy
67	13 24 28.46	-43 14 56.3	-	-	PC
122	13 24 29.70	-43 02 06.4	-	-	PC
43/44	13 24 30.86	-42 52 40.8	35527 ^a	70	galaxy

Table 2—Continued

ID	R.A. (J2000)	Dec. (J2000)	v_r (km s ⁻¹)	$\sigma(v_r)$ (km s ⁻¹)	Comments
117	13 24 34.38	-42 57 32.4	-	-	PC
127	13 24 34.61	-43 12 50.5	7717	194	galaxy
133	13 24 35.30	-43 06 15.4	-	- ^b	PC
119	13 24 48.71	-42 52 35.5	-	-	PC
298	13 25 01.09	-42 48 21.9	-	-	PC
136	13 25 01.16	-43 11 59.0	-	- ^b	PC
299	13 25 01.29	-42 54 26.5	2544	92	galaxy
132	13 25 23.45	-42 53 26.2	2017	78	galaxy
108	13 25 25.73	-43 05 16.6	-	-	PC
103	13 25 28.72	-42 50 12.3	-	-	PC
314	13 25 37.53	-42 55 33.5	-	-	PC
116	13 25 39.63	-43 04 01.4	32124	253	galaxy
123	13 25 41.37	-43 12 12.6	31018	230	galaxy
317	13 25 45.63	-43 01 15.5	5850	91	galaxy
72	13 25 49.23	-43 00 02.2	7349	87	galaxy
90	13 25 49.26	-43 02 20.4	9942	113	galaxy
135	13 25 49.95	-43 02 26.3	38298	114	galaxy
107	13 25 56.63	-42 58 45.5	-	-	PC
101	13 26 02.24	-43 08 55.7	- ^a	-	PC
109/110	13 26 02.23	-43 17 34.8	- ^a	-	PC
134	13 26 17.27	-43 06 39.3	24742	79	galaxy
113	13 26 21.29	-42 57 19.1	-	-	PC
125	13 26 23.64	-43 00 45.6	-	-	PC
100	13 26 50.44	-42 50 36.4	-	- ^b	PC

^aMeasured in both fields; the radial velocity is the average.

^bRegions of spectrum ignored during correlation to remove spikes, leading to high uncertainties.

^cPC denotes a poor correlation of the object to the GC template spectrum.

Table 3. Radial Velocity Measurements for Previously Known Globular Clusters

Cluster	RA (J2000)	Dec. (J2000)	R_{gc} (arcmin)	V (mag)	(C-T ₁)	v_r (km s ⁻¹)	$\sigma(v_r)$ (km s ⁻¹)
C2	13 24 51.47	-43 12 11.2	12.86	18.38	1.546	606 ^a	38
C3	13 24 58.21	-42 56 10.0	7.33	17.68	1.940	559	20
C4	13 25 01.81	-43 09 25.5	9.53	17.88	1.451	687	49
C6	13 25 22.19	-43 02 45.6	1.89	16.83	-	846 ^a	18
C7	13 26 05.40	-42 56 32.4	8.30	16.90	1.533	599	15
C10	13 24 48.04	-43 08 14.3	10.13	18.30	1.727	856	33
C11	13 24 54.70	-43 01 21.6	6.02	17.67	2.011	765	15
C13	13 25 06.22	-43 15 11.6	14.58	18.48	1.703	599 ^a	25
C14	13 25 10.49	-42 44 52.8	16.56	17.75	1.655	691 ^a	19
C15	13 25 30.39	-43 11 49.6	10.69	18.43	1.881	672	33
C17	13 25 39.72	-42 55 59.1	5.62	17.49	1.422	785	18
C18	13 25 39.86	-43 05 01.8	4.48	17.29	1.603	476 ^a	19
C19	13 25 43.38	-43 07 22.9	6.87	17.87	0.324	607 ^a	18
C20	13 25 49.68	-42 54 49.3	7.50	17.89	1.472	745 ^a	16
C21	13 25 52.73	-43 05 46.5	6.52	17.62	1.576	461	96
C26	13 26 15.25	-42 48 29.4	15.36	17.94	2.068	370 ^a	21
C30	13 24 54.35	-42 53 24.7	9.84	17.05	1.788	786	17
C32	13 25 03.37	-42 50 46.1	11.29	18.22	2.006	708	32
C33	13 25 16.26	-42 50 53.3	10.47	18.67	-	520	41
C36	13 26 07.73	-42 52 00.2	11.72	18.24	1.378	696	43
C37	13 26 10.57	-42 53 42.7	10.81	18.17	1.691	612 ^a	21
C38	13 26 23.77	-42 54 01.1	12.50	18.34	1.544	397 ^a	23
C39	13 26 42.00	-43 07 44.9	15.11	17.28	1.647	247	26
C44	13 25 31.73	-43 19 22.8	18.25	18.48	1.441	515 ^a	43
C47	13 25 49.94	-42 52 09.3	9.88	18.80	1.402	592	34
C48	13 25 49.83	-42 50 15.1	11.63	18.65	1.281	557	77
C50	13 26 19.64	-43 03 18.6	9.75	18.59	1.633	605	90
G271	13 25 13.94	-42 57 42.5	4.25	18.80	1.092	263	98
G342	13 25 05.75	-42 59 00.3	4.53	18.20	-	565	37
G369	13 24 57.49	-42 59 23.3	5.78	18.80	1.436	527	58
pff_gc-018	13 24 47.08	-43 06 01.7	8.87	18.91	1.603	554	44

Table 3—Continued

Cluster	RA (J2000)	Dec. (J2000)	R_{gc} (arcmin)	V (mag)	(C-T ₁)	v_r (km s ⁻¹)	$\sigma(v_r)$ (km s ⁻¹)
pff_gc-041	13 25 11.14	-43 03 09.6	3.62	19.61	1.471	432	179
pff_gc-042	13 25 12.19	-43 16 33.7	15.67	18.97	1.352	678	87
pff_gc-056	13 25 32.80	-42 56 24.3	4.84	18.64	1.286	275 ^a	44
pff_gc-058	13 25 35.12	-42 56 45.1	4.60	18.68	1.259	376	78
pff_gc-060	13 25 42.42	-42 59 02.5	3.43	18.93	1.634	818 ^c	96
pff_gc-064	13 25 43.89	-42 50 42.5	10.85	19.80	1.758	556 ^{a,c}	63
pff_gc-073	13 25 52.76	-42 58 41.6	5.21	20.10	1.759	470	189 ^b
pff_gc-075	13 25 53.47	-43 03 56.6	5.49	19.61	1.768	764	59
pff_gc-076	13 25 53.74	-43 19 48.5	19.26	19.07	1.923	351	39
pff_gc-083	13 26 01.81	-42 58 15.0	6.89	20.04	1.683	473	53
pff_gc-085	13 26 06.39	-43 00 38.1	7.11	19.63	1.262	469	108
pff_gc-089	13 26 20.19	-43 10 35.7	13.48	18.95	1.324	553	103

^aMeasured in both fields; the radial velocity listed is the average.

^bRegions of spectrum affected by cosmic ray spikes were masked out during correlation.

^cStrong secondary correlation peaks.

Table 4. Previously Known Clusters in HHG04 Candidate List

Candidate ID	Cluster
9	C18
12	C3
16	C14
30	C2
42	pff_gc-056
48	pff_gc-060
82	pff_gc-041
83	pff_gc-075
85	pff_gc-085
95	pff_gc-064
111	pff_gc-083
118	pff_gc-073

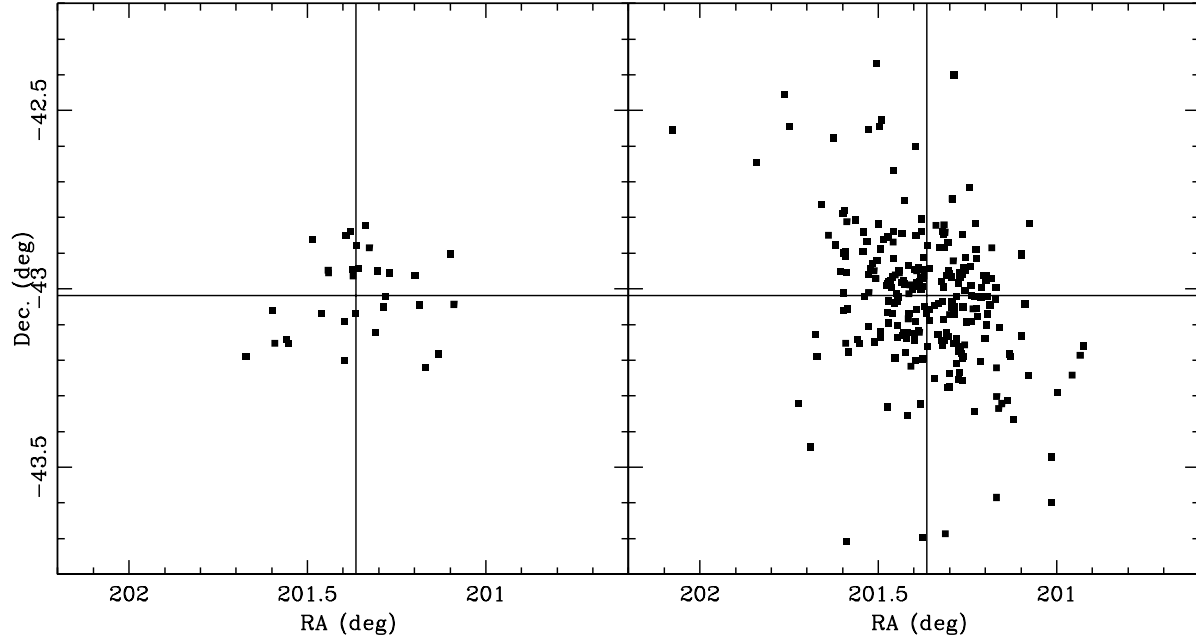


Fig. 1.— The positions in RA and Dec: (*left*) the 31 new globular clusters found in this study; (*right*) 215 known globular clusters from previous literature (Peng, Ford, and Freeman 2004). The cross hairs indicate the centre of the galaxy.

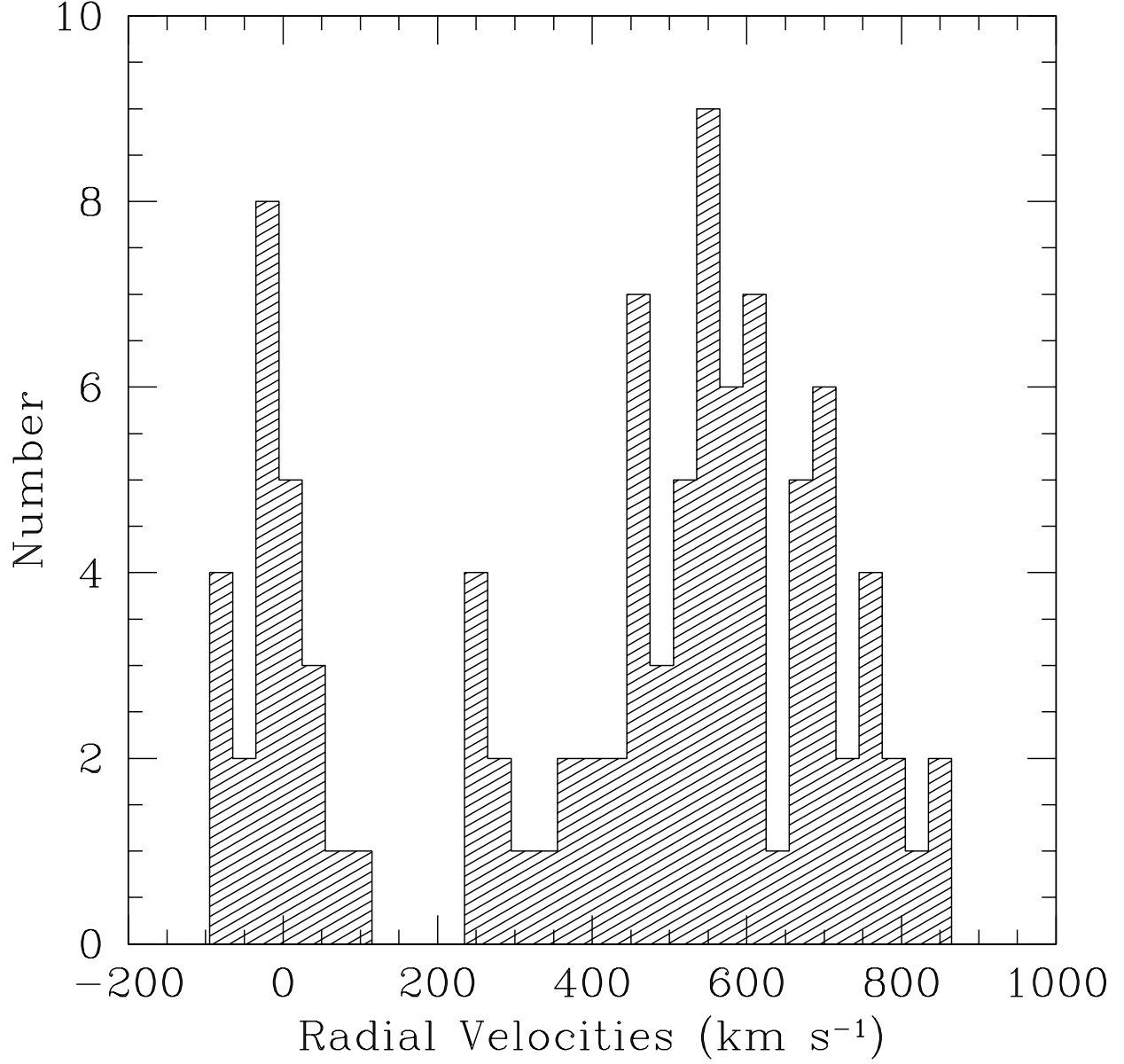


Fig. 2.— The velocity distribution of the 74 measured GCs ($v_r \sim 200$ to 900 km s^{-1}) and foreground stars ($v_r \sim -90$ to 110 km s^{-1}).

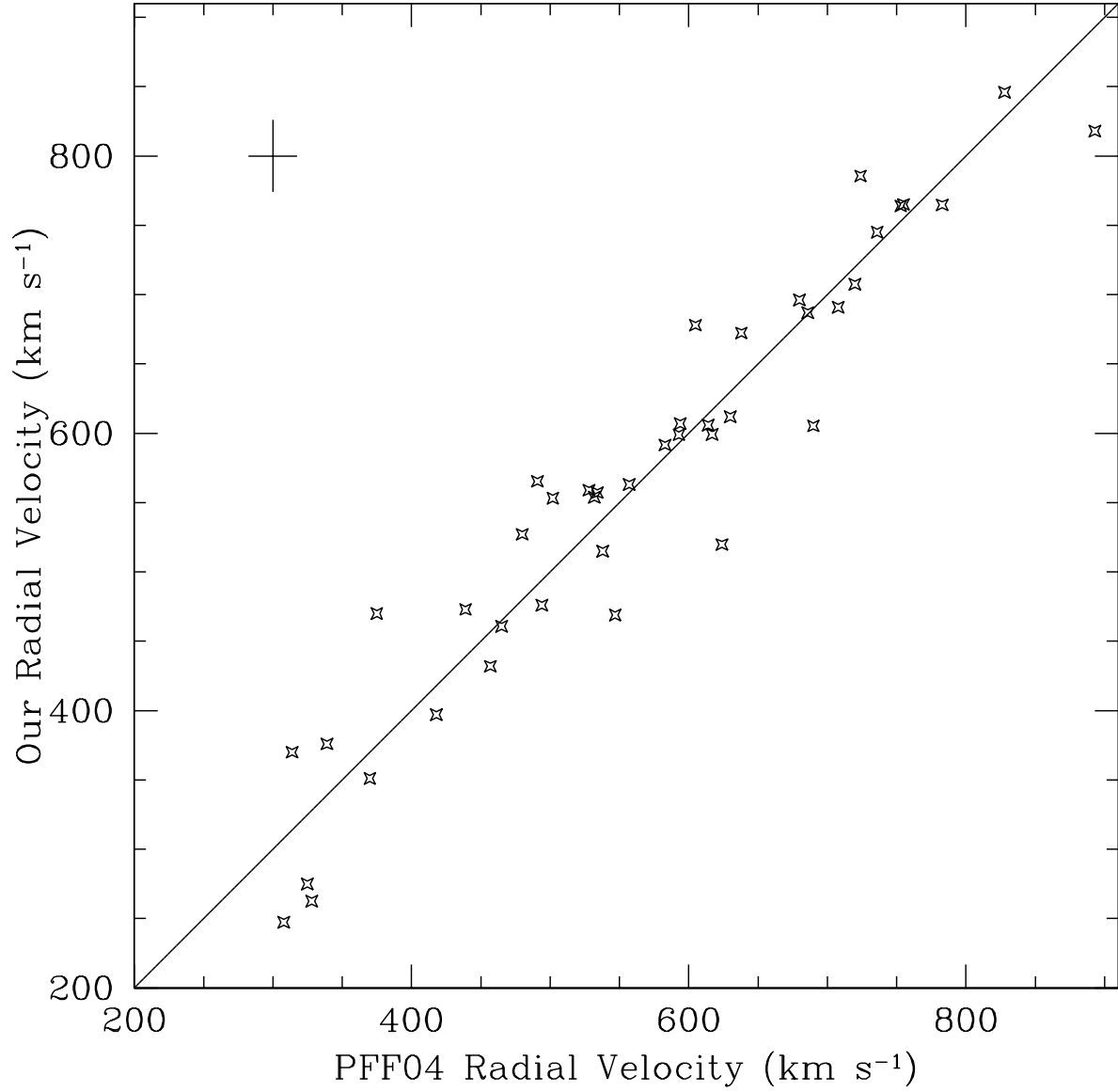


Fig. 3.— Comparison of our radial velocity to the PFF04 radial velocity for the 42 known clusters in common (excluding C10; see text). The standard deviation of the differences is ± 44.5 km s⁻¹. The average internal uncertainty of each set of measurements is shown in the upper left of the plot.

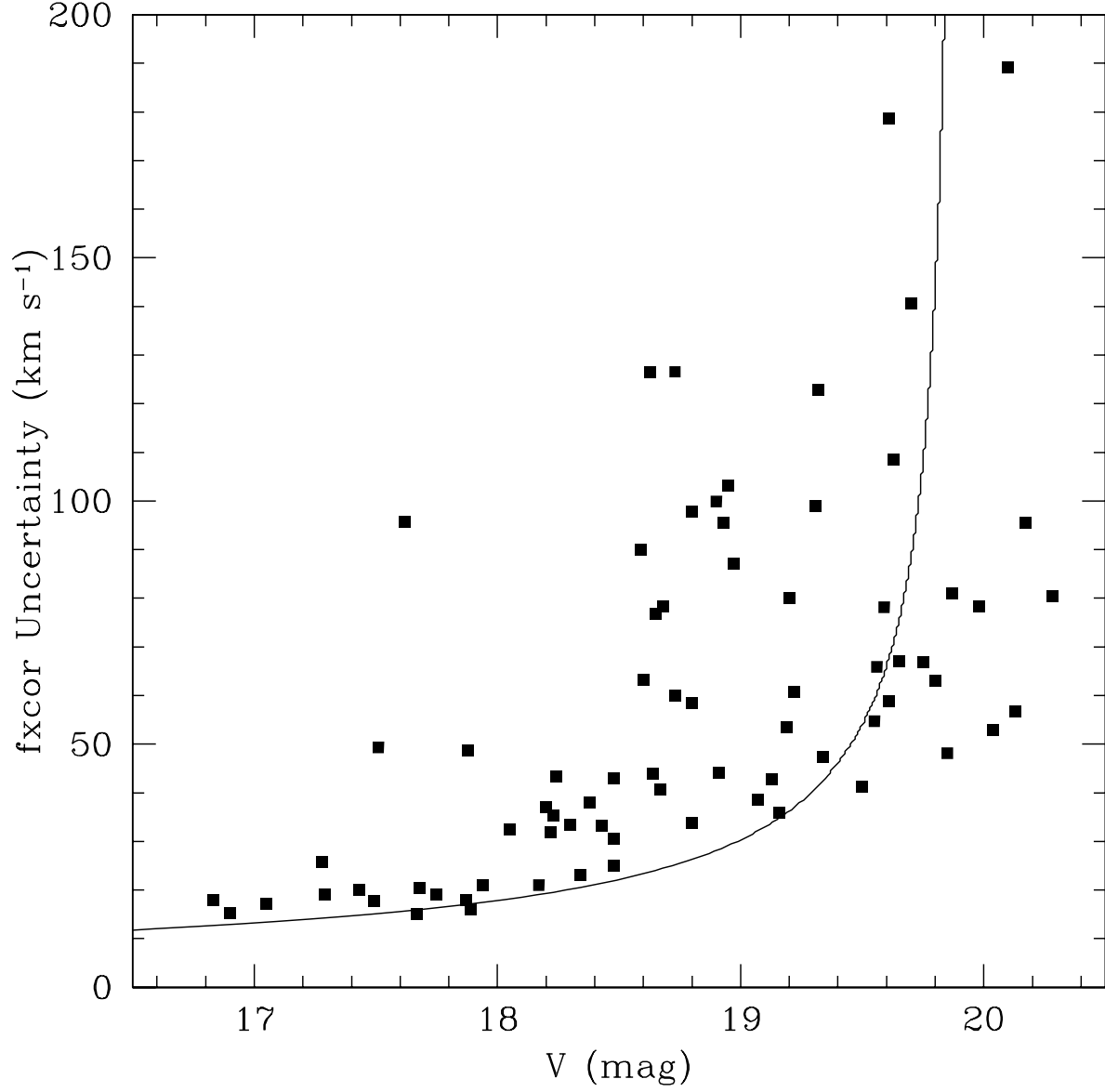


Fig. 4.— The *fxcor* velocity uncertainties obtained for the 74 globular clusters listed in Tables 1 & 3, compared to their V magnitudes. The solid line is the ideally expected increase in velocity uncertainty with increasing V magnitude, based on the *mknoise* simulations.

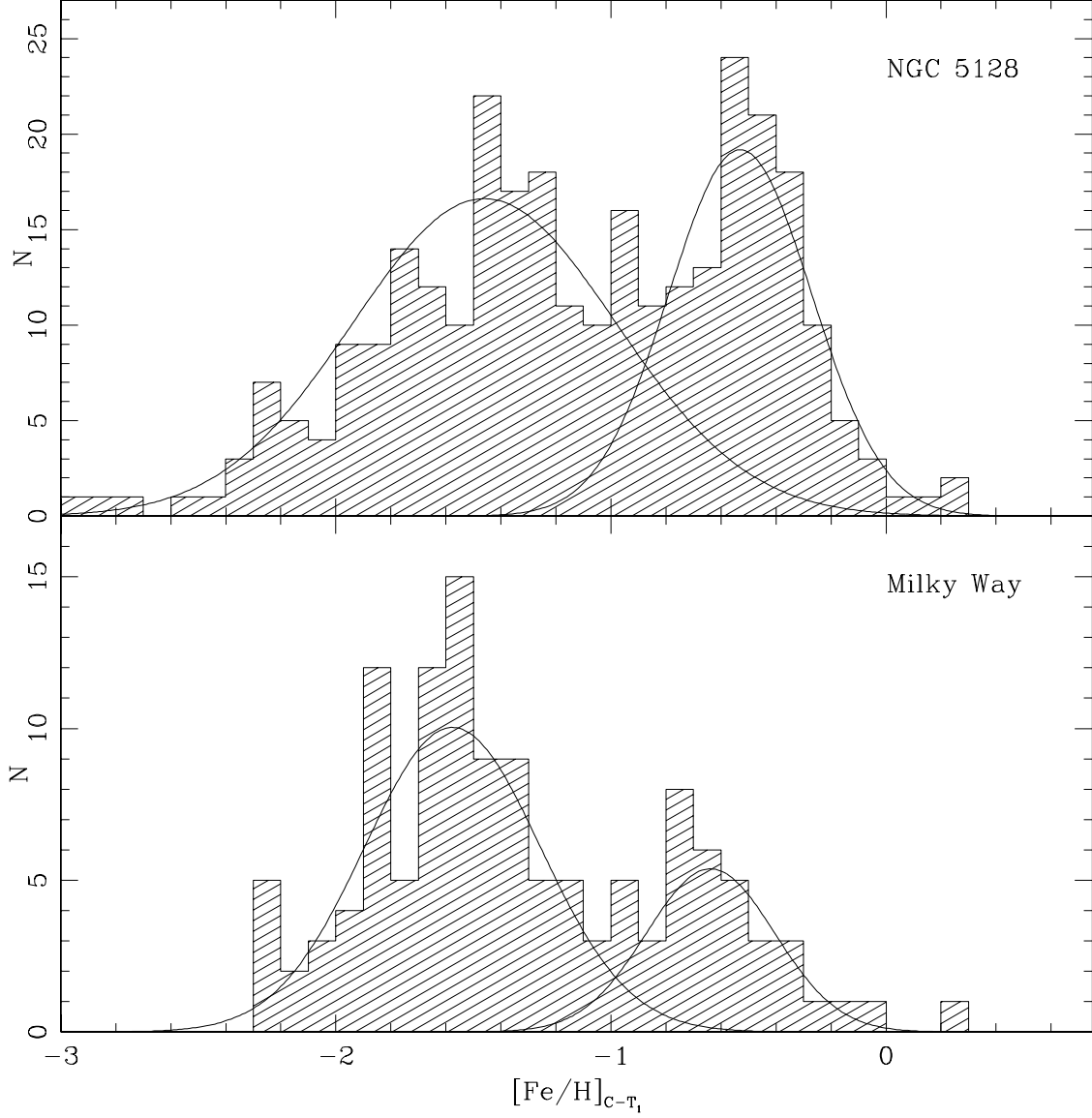


Fig. 5.— *Top*: The metallicity distribution function for 299 GCs including the 31 new GCs from this survey. The distribution is fit with two Gaussians with centroids at $[\text{Fe}/\text{H}] = (-1.46, -0.53)$ and standard deviations $(0.54, 0.30)$. *Bottom*: The metallicity distribution function for 148 Milky Way GCs with Gaussian centroids at $[\text{Fe}/\text{H}] = (-1.58 \pm 0.05, -0.64 \pm 0.07)$ and standard deviations $(0.32, 0.23)$

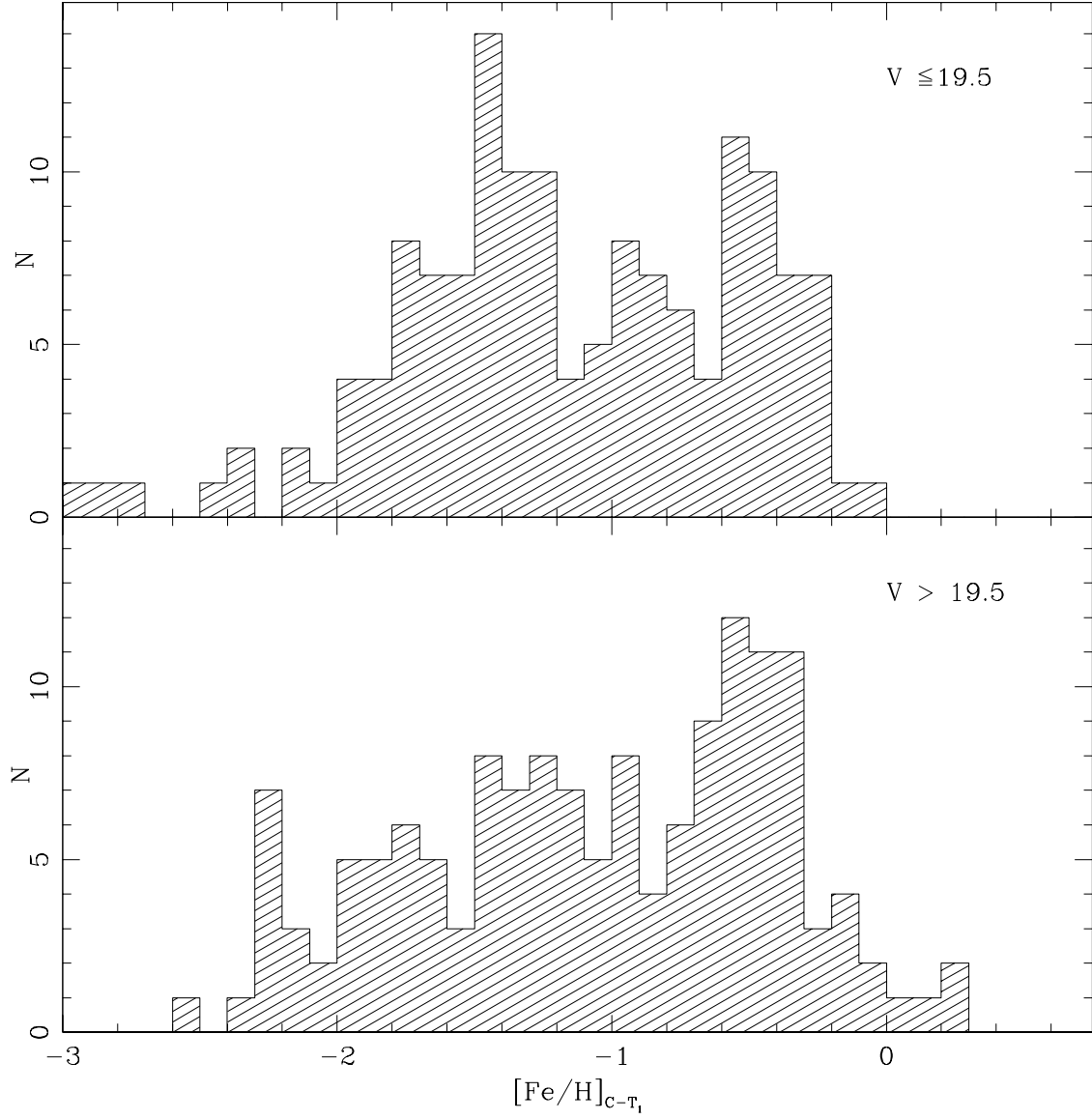


Fig. 6.— The metallicity distributions for the 299 GCs divided in V magnitude; *top*: 147 GCs with $V \leq 19.5$ mag and *bottom*: 152 GCs with $V > 19.5$ mag.

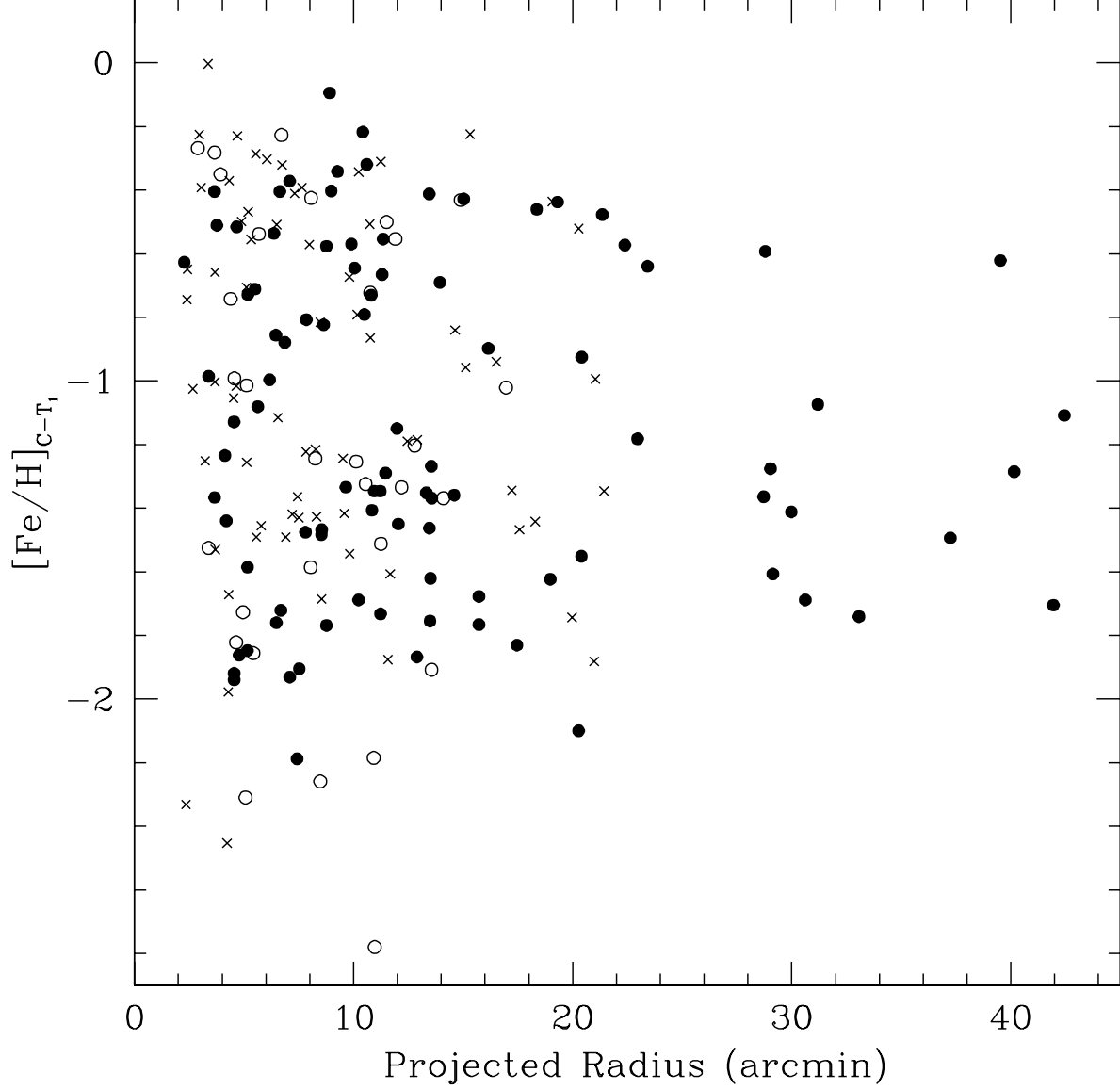


Fig. 7.— Metallicity from the C-T₁ colour index vs. projected galactocentric distance for the radial-velocity confirmed GCs. The *crosses* denote clusters from Harris et al. (1992); van den Bergh, Hesser, & Harris (1981); Hesser, Harris, & Harris (1986), the *solid circles* are clusters from Peng, Ford, & Freeman (2004), and the *open circles* are new clusters from this study.